# Macroscopic model of rotating nuclei

Arnold J. Sierk*
*Physics Division, Oak Ridge National Laboratory, Oak Ridge, Tennessee 37830*
*and Theoretical Division, Los Alamos National Laboratory, Los Alamos, New Mexico 87545*
(Received 19 December 1985)

I present a macroscopic model for the energy of rotating nuclei which has several refinements relative to the rotating-liquid-drop model. Of most importance are the inclusion of finite-range effects in the nuclear surface energy by means of a Yukawa-plus-exponential potential, finite surface diffuseness effects in the Coulomb energy and in the rotational moments of inertia, and an improved specification of nuclear shapes. With this model I calculate the properties of points of equilibrium corresponding to nuclear ground states and fission saddle points. The results are qualitatively similar to those of the rotating-liquid-drop model, but there are significant quantitative differences in fission-barrier heights and moments of inertia. Fission barriers for nonrotating nuclei are calculated for nuclei with atomic numbers varying from 14 to 117. For rotating nuclei, detailed results are given for the entire range of angular momentum for which a fission barrier exists, for nuclei with atomic numbers from 20 to 100, and for mass numbers which exceed the range of known nuclei. The calculated barriers are lower than liquid-drop-model barriers for lighter nuclei and are consistent with those deduced from experimental fission-fusion data over a wide range of nuclear species. The present calculations indicate that super-deformed rotating ground states, which are predicted in the liquid-drop model, would not survive fission long enough to undergo electromagnetic decay. Multiparameter functions which approximately reproduce the calculated results for barrier heights and moments of inertia are described.

## I. INTRODUCTION

When heavy nuclei are collided at sufficiently high energies, composite systems are formed which may have angular momenta in excess of $100\hbar$, where $\hbar$ is Planck's constant divided by $2\pi$. When considering systems with such large angular momenta, it is important to know whether a locally stable equilibrium configuration of the fused nuclei exists, because an equilibrated compound nucleus will not be formed if such a configuration does not exist. After formation of a compound nucleus, the height of the fission barrier strongly affects the probability of fission decay relative to other decay channels. In addition, the moments of inertia of the saddle-point configuration may determine the angular distribution of fission fragments.

The rotating-liquid-drop model[1] has provided a simplified model of the potential energies and equilibrium configurations of rotating nuclei. However, when the liquid-drop model, with the best available constants[2] and a statistical deexcitation model, is used to reproduce experimental data on heavy-ion-induced fission and evaporation-residue formation, the fission-barrier heights used must be reduced from liquid-drop values[1] by a factor which has been reported to be between about 0.5 and 0.9, for nuclei with mass numbers less than about 200.[3–16]

Since the last determination of parameters in the liquid-drop model,[2] an improved semiempirical mass formula has been developed,[17] in which the surface energy of the liquid-drop model is replaced by the Yukawa-plus-exponential nuclear energy,[18] the effect of the diffuseness of the surface of the nuclear charge distribution on the Coulomb energy is included,[19] and various other physical effects are modeled.[17] In addition to the effects mentioned, the diffuseness of the surface of the nuclear matter distribution changes the rotational moments of inertia from their liquid-drop-model values.[19] Finally, the existing calculations using the rotating-liquid-drop model have only approximately included the effects of triaxiality.[1]

Nuclear systems with large amounts of angular momentum which are formed in heavy-ion collisions will generally also have high internal excitation energy. For sufficiently high internal energies, shell and pairing effects vanish, and a macroscopic model may be reasonable. For systems with small amounts of internal energy and also low macroscopic fission barriers (for example, actinide nuclei), single-particle effects do play an important role. However, a macroscopic model with the correct global behavior should provide both a good representation of the fission properties of highly excited lighter nuclei and a baseline model against which to compare experimental results in order to determine when single-particle effects are important.

In this paper I present a macroscopic model of rotating nuclei which incorporates the following changes relative to the liquid-drop model:

(1) The surface energy of the liquid-drop model is replaced by the Yukawa-plus-exponential nuclear energy, which models effects of the finite range of the nuclear force, nuclear saturation, and the finite surface thickness of real nuclei;[18]

(2) The Coulomb energy is calculated for a charge distribution with a realistic surface diffuseness;[19]

(3) The rotational moments of inertia are calculated for

 ©1986 The American Physical Society

rigidly rotating nuclei with realistic surface density profiles;[19]

(4) The parameters of the model for the various contributions to the energy of the nucleus provide a better fit than do those of the liquid-drop model to nuclear ground-state masses and fission barriers of nonrotating nuclei;[17,18]

(5) A flexible shape parametrization is used which allows accurate estimation of the convergence of results as a function of the number of degrees of freedom of the nuclear shapes considered;[20]

(6) Accurate modeling of the triaxial nuclear shapes occurs; and

(7) A precise calculation is made of the value, slope, and curvature of the potential-energy surface by means of numerical quadrature.

Of the above items, those numbered (1)—(4) and (6) have been included in a previous calculation.[21] However, due to the restricted shape parametrization, and to approximations used to locate the saddle point in Ref. 21, those results have significant quantitative differences from those reported here, in some cases.[14]

In Sec. II, I present the ingredients of the model, in Sec. III, I give a description of the qualitative results of calculations in the model, and in Sec. IV, I discuss detailed results for specific nuclei and a method for reliably approximating all results in order to have a practical way of determining fission barrier heights and moments of inertia for any nucleus as a function of angular momentum. Section V is a discussion and summary of the calculations. In several Appendices, I discuss some details of the calculations and their accuracy.

## II. INGREDIENTS OF THE MODEL

### A. The rotating-liquid-drop model

Because of its simplicity, and in order to facilitate later comparisons, I will first review the properties of the rotating-liquid-drop model.[1] There are three important contributions to the potential energy of deformation: a surface tension energy (arising from saturating, short-range nuclear forces) which tends to minimize the surface area of the nucleus, a repulsive Coulomb energy (arising from mutual repulsion of protons) which tends to distort or disrupt the nucleus, and angular momentum, which also favors disruption because large moments of inertia are energetically favored. The nucleus is assumed to be formed of an incompressible fluid with a constant charge density and a sharp surface, which rotates as a rigid body. Energies are often expressed in units of the surface energy of the nonrotating spherical ground state,

$$E_s^{(0)}=a_s^{\mathrm{LD}}A^{2/3}(1-\kappa_s^{\mathrm{LD}}I^2)\ , \tag{1}$$

where $a_s^{\mathrm{LD}}$ and $\kappa_s^{\mathrm{LD}}$ are the liquid-drop-model surface-energy and surface-asymmetry constants, respectively, $I\equiv(N-Z)/A$ is the neutron-proton asymmetry, and $N$, $Z$, and $A$ are the neutron, proton, and nucleon numbers of the nucleus, respectively. The unit of distance is

$$R_0=r_0^{\mathrm{LD}}A^{1/3}\ , \tag{2}$$

while the mass unit is

$$M_0=m_0^{\mathrm{LD}}A\ , \tag{3}$$

and $r_0^{\mathrm{LD}}$ and $m_0^{\mathrm{LD}}$ are the liquid-drop radius and the nuclear-mass constants, respectively. The best existing liquid-drop-model fit to nuclear masses and fission barriers gives:[2]

$$a_s^{\mathrm{LD}}=17.9439\ \mathrm{MeV}\ ,$$

$$\kappa_s^{\mathrm{LD}}=1.7826\ ,$$

$$r_0^{\mathrm{LD}}=1.2249\ \mathrm{fm}\ ,$$

and

$$m_0^{\mathrm{LD}}c^2=939.15\ \mathrm{MeV}\ , \tag{4}$$

where $c$ is the speed of light in a vacuum.

If I denote by $L$ the magnitude of angular momentum in units of $\hbar$, the rotational energy of the sphere is

$$E_R^{(0)}=\hbar^2L^2/2I_0\ , \tag{5}$$

where $I_0=\frac{2}{5}M_0R_0^2$ is the moment of inertia of a rigid sphere. The electrostatic energy of the sphere is

$$E_C^{(0)}=\frac{3}{5}\frac{Z^2e^2}{R_0}\ , \tag{6}$$

where $e$ is the magnitude of the charge of an electron. It is possible to consider all results as functions of two parameters:[1] the fissility parameter

$$x\equiv\frac{E_C^{(0)}}{2E_s^{(0)}}=\frac{Z^2/A}{50.88(1-\kappa_s^{\mathrm{LD}}I^2)}\ , \tag{7}$$

and the rotational energy parameter

$$y\equiv\frac{E_R^{(0)}}{E_s^{(0)}}=\frac{1.9249}{(1-\kappa_s^{\mathrm{LD}}I^2)}\frac{L^2}{A^{7/3}}\ . \tag{8}$$

The fissility parameter varies from 0 to 1 for beta-stable nuclei whose charge numbers vary from 0 to about 120 (where the macroscopic fission barrier vanishes). For a nucleus with $Z=80$, $A=200$, $L=80\hbar$, $y$ is approximately 0.057.

The deformation energy may be expressed as

$$E_{\mathrm{tot}}^{\mathrm{LD}}=B_s^{\mathrm{LD}}E_s^{(0)}+B_C^{\mathrm{LD}}E_C^{(0)}+B_R^{\mathrm{LD}}E_R^{(0)}\ , \tag{9}$$

where $B_s^{\mathrm{LD}}$, $B_C^{\mathrm{LD}}$, and $B_R^{\mathrm{LD}}$ are the dimensionless surface, Coulomb, and rotational energy functionals, respectively. Usually, the energy is expressed relative to that of the spherical, nonrotating ground state

$$V^{\mathrm{LD}}/E_s^{(0)}=B_s^{\mathrm{LD}}-1+2x(B_C^{\mathrm{LD}}-1)+yB_R^{\mathrm{LD}}\ . \tag{10}$$

The energy functionals have the form

$$B_s^{\mathrm{LD}}=\frac{1}{4\pi R_0^2}\oint dS\ , \tag{11}$$

$$\frac{32\pi^2B_C^{\mathrm{LD}}}{15}=\int d^3r\int d^3r'\frac{1}{\sigma}$$
$$=-\tfrac{1}{6}\oint dS\oint dS'\frac{d\mathbf{S}\cdot\boldsymbol{\sigma}\,d\mathbf{S}'\cdot\boldsymbol{\sigma}}{\sigma}\ , \tag{12}$$

and

$$B_R = I_0 \left[ \frac{3}{4\pi} \int d^3r \, r_\perp^2 \right]^{-1} . \tag{13}$$

All integrals are taken over the entire nuclear surface or volume. $d\mathbf{S}$ and $d\mathbf{S}'$ are the vector surface elements of the nuclear surface, $\boldsymbol{\sigma} = \mathbf{r} - \mathbf{r}'$, $\sigma = |\boldsymbol{\sigma}|$, and $r_\perp$ is the perpendicular distance from the point described by the vector $\mathbf{r}$ to the rotation axis of the nucleus. The second form of Eq. (12) is derived from the first by twice applying Gauss's divergence theorem.[22]

### B. Yukawa-plus-exponential nuclear energy

The surface energy of the liquid-drop model suffers from several deficiencies in attempting to describe real nuclei. Perhaps the most important of these is the neglect of proximity effects; that is, there is in the liquid-drop model an unrealistically high surface energy for strongly deformed shapes, and an absence of attraction between separated nuclei. One method for improved modeling of the macroscopic nuclear energy is the Yukawa-plus-exponential double-folding potential.[18] The generalized nuclear energy is a double volume integral of an empirical Yukawa-plus-exponential folding function. With this technique, using one additional parameter relative to the liquid-drop model (the range of the potential), one can describe heavy-ion scattering potentials, fusion barriers for light and medium-mass nuclei, the lower (than liquid drop) fission barriers observed in nuclei with $A \leqq 200$, and also satisfy the condition of nuclear saturation.[17,18]

If the constants $r_0$, $a_s$, and $\kappa_s$ are defined analogously to those in the liquid-drop model, and in addition I introduce

$$c_s \equiv a_s(1 - \kappa_s I^2) , \tag{14}$$

the Yukawa-plus-exponential nuclear energy may be written as

$$E_n = -\frac{c_s}{8\pi^2 r_0^2 a^3} \int d^3r \int d^3r' \left( \frac{\sigma}{a} - 2 \right) \frac{e^{-\sigma/a}}{\sigma} . \tag{15}$$

Just as in Eqs. (11)–(13), the integrals are over the volume of a sharp-surfaced nucleus. The range $a$ is the one additional parameter of this modification of the liquid-drop model. The value of $r_0$ is determined from average charge radii of nuclei found in electron-scattering experiments,[17,18] $a$ is determined from heavy-ion scattering experiments,[18] while $a_s$ and $\kappa_s$ are determined from fitting the macroscopic fission barriers of nuclei with mass numbers from 109 to 252 at low angular momentum.[17] The values of the constants used here are

$$r_0 = 1.16 \text{ fm} ,$$

$$a = 0.68 \text{ fm} ,$$

$$a_s = 21.13 \text{ MeV} ,$$

$$\kappa_s = 2.3 ,$$

and

$$M_0 c^2 = 931.5016A - 0.511\,004Z \text{ MeV} . \tag{16}$$

The units of energy and length are defined by equations analogous to Eqs. (1) and (2).

The integrals in Eq. (15) can be performed analytically for a sphere to lead to a form which makes clearer the relationship to the liquid-drop model[18]

$$E_n^{(0)} = \left\{ 1 - 3\left( \frac{a}{R_0} \right)^2 + \left( \frac{R_0}{a} + 1 \right) \left[ 2 + 3\frac{a}{R_0} + 3\left( \frac{a}{R_0} \right)^2 \right] \times e^{-2R_0/a} \right\} E_s^{(0)} , \tag{17}$$

Note that the lowest-order modification to the liquid-drop model is to reduce the nuclear energy, which is the principal reason why $a_s$ is larger than $a_s^{\mathrm{LD}}$. Equation (15) may also be transformed to a double surface integral by twice applying Gauss's divergence theorem.[18,19] For axially symmetric shapes, one of the resulting angular integrations may be performed trivially, leading to a three-dimensional integral, while for triaxial shapes a four-dimensional integral remains. These integrals are approximated by use of Gaussian-Legendré quadrature formulas. When calculating equilibrium configurations, it is also necessary to know the first and second derivatives of the energy with respect to the shape coordinates. These derivatives are calculated by first differentiating the surface-integral expressions for the energy (with the derivatives of the end points being properly taken into account), and then making Gaussian quadrature approximations to the resulting integrals[20,22] (see Appendix A).

### C. Coulomb energy

For a charge distribution made diffuse by folding a Yukawa function with range $a_c$ over a liquid-drop distribution, the Coulomb energy functional may be written as

$$B_C = B_C^{\mathrm{sharp}} + \Delta B_C , \tag{18}$$

where $B_C^{\mathrm{sharp}}$ is given by Eq. (12), and[19]

$$\frac{32\pi^2}{15} \Delta B_C = -\int d^3r \int d^3r' \left( 1 + \frac{\sigma}{2a_c} \right) \frac{e^{-\sigma/a_c}}{\sigma} . \tag{19}$$

Equation (19) has the same form as Eq. (15), except for a different relative sign between the two terms in parentheses. The leading order term in $\Delta B_C$ is of the order $a_c^2/R_0^2$ and is shape independent, while the term of order $a_c^3/R_0^3$ has the same shape dependence as $B_s$.[19] In effect, ignoring effects of $\Delta B_C$ results in a renormalization of the constants $r_0$ and $a_s$, which is one of the reasons why the liquid-drop model has such a large value for $r_0$ [Eq. (4)].[2]

The surface-integral form for $B_C^{\mathrm{sharp}}$ may be expressed for axially symmetric shapes as a two-dimensional integral whose integrand contains complete elliptic integrals.[22] For triaxial shapes, a four-dimensional integral remains. First and second derivatives of the Coulomb energy with respect to shape coordinates are calculated in a similar manner to those for the Yukawa-plus-exponential

energy (see Appendix A). The range parameter $a_c$ is chosen to reproduce a surface-width parameter, as defined by Myers[23] and Süssmann,[24] of 0.99 fm, which gives

$$a_c = 0.704 \text{ fm} . \tag{20}$$

### D. Rotational energy

For an isolated nucleus, the rotational energy is given by

$$E_R = \frac{L^2 \hbar^2}{2I} , \tag{21}$$

where $I$ is the largest of the principal-axis moments of inertia. For a matter distribution made diffuse by folding a Yukawa function over a sharp-surfaced one, as discussed in the preceding subsection, the moment of inertia has a particularly simple form[19]

$$I = I^{\text{sharp}} + 4M_0 a_M^2 , \tag{22}$$

where $I^{\text{sharp}}$ is defined by the denominator of Eq. (13), and $a_M$ is the range parameter of the folding function. I use the same diffuseness parameter for both the charge and matter distribution, or

$$a_M = a_c = 0.704 \text{ fm} . \tag{23}$$

The volume integral in Eq. (13) may be transformed to a surface integral, which leads to a one-dimensional integral for axially symmetric shapes,[20] or to a two-dimensional integral for triaxial shapes. First and second derivatives of the rotational energy are calculated in a similar manner to those for the nuclear and Coulomb energies (see Appendix A).

### E. Shape parametrization

For the majority of the results presented here, I use a triaxial generalization of the Legendré-polynomial parametrization of Ref. 20. First consider shapes which are axially symmetric, reflection symmetric about a plane perpendicular to the symmetry axis, and whose surface may be specified in cylindrical coordinates $(\rho,\phi,z)$ as[20]

$$(\rho_s^0)^2 = \sum_{k=0}^{N_z} a_{2k} P_{2k}(z/z_0) . \tag{24a}$$

$z$ is the coordinate along the symmetry axis, $2z_0$ is the length of the nucleus along the $z$ axis, $\rho_s^0$ is the radial coordinate of the nuclear surface, and $P_{2k}$ is an ordinary Legendré polynomial. Defining $x \equiv z/z_0$ and imposition of volume conservation leads to[20]

$$(\rho_s^0)^2 = \sum_{k=1}^{N_z} a_{2k}[P_{2k}(x) - 1] , \tag{24b}$$

and to a specification of $z_0$ in terms of the $a_{2k}$'s. I will subsequently use the notation $\sum_k$ to mean $\sum_{k=1}^{N_z}$. There are $N_z$ independent parameters to describe an axially symmetric shape, $\{a_2, a_4, \ldots, a_{2N_z}\}$. This form of shape parametrization allows an accurate description of nearly spherical shapes, as well as elongated shapes, and shapes with one or more necks.[20] Shapes with cusps, for example tangent spheroids, cannot be accurately described without taking a very large value for $N_z$. However, this is not usually a serious deficiency when using finite-range energy functionals, as I do here.

In order to describe triaxial shapes, I use a generalization of Eq. (24),

$$\rho_s(z,\phi) = \rho_s^0(z) \frac{\eta(\phi,z)}{\lambda(z)} , \tag{25}$$

where

$$\eta(\phi,z) = 1 + [\alpha_1 - \tfrac{3}{2}\alpha_3(1-x^2)] P_2(\cos\phi) + [\alpha_2 - \tfrac{3}{2}\alpha_4(1-x^2)] P_4(\cos\phi) \tag{26a}$$

and

$$\lambda(z) = 1 + \tfrac{1}{4}[\alpha_1 - \tfrac{3}{2}\alpha_3(1-x^2)] + \tfrac{9}{64}[\alpha_2 - \tfrac{3}{2}\alpha_4(1-x^2)] . \tag{27a}$$

The four parameters $\{\alpha_1, \ldots, \alpha_4\}$ define the amount of deviation from axial symmetry. By allowing them to vary freely in a number of ground-state and saddle-point calculations, I find that $\alpha_3$ and $\alpha_4$ are not needed to describe the equilibrium shapes of rotating nuclei, so they are set to zero for all results presented in this paper. This simplification leads to

$$\eta(\phi,z) = 1 + \alpha_1 P_2(\cos\phi) + \alpha_2 P_4(\cos\phi) = \eta(\phi) \tag{26b}$$

and

$$\lambda = 1 + \alpha_1/4 + 9\alpha_2/64 . \tag{27b}$$

I will use the notation $q_i$ to denote the vector whose components are

$$\{a_2, a_4, \ldots, a_{2N_z}, \alpha_1, \alpha_2\} ,$$

and $N_c$ to denote the number of independent coordinates:

$$\begin{aligned} N_c &= N_z \quad \text{for axial symmetry} , \\ N_c &= N_z + 2 \quad \text{for triaxiality} . \end{aligned} \tag{28}$$

Nearly all of the results in this paper are for $N_z = 5$, so triaxial shapes have seven degrees of freedom.

In addition to the previously mentioned difficulty in describing shapes with cusps, the Legendré-polynomial parametrization suffers, in common with many other highly flexible parametrizations, another difficulty when used with finite-range forces. For very light nuclei, small protuberances may appear on equilibrium shapes. The physical mechanism is that distortions of the surface on a scale smaller than $a/R_0$ (which varies as $A^{-1/3}$) will lower the Coulomb energy, but not appreciably raise the nuclear energy.[18] This difficulty is manifested in the present calculations by the appearance of two saddle points for nuclei with $Z \leq 50$. One saddle has pointed ends, and lies $\sim 0.2$ MeV lower in energy than the true saddle point, while the other has excessively flattened ends and lies $\sim 0.5$ MeV too high in energy. For these lighter nuclei, and for those with very small necks, I employ the three-quadratic-surface shape parametrization,[25] in which nuclear shapes are described by smoothly joined portions of three concoids of revolution. This parametrization has three independent coordinates for mass-symmetric shapes.

It is less accurate than the Legendré-polynomial parametrization for shapes that are close to a single spheroid or sphere,[20,25] but the discrepancy in energy for saddle points in the Yukawa-plus-exponential model is no more than 0.1 MeV for nuclei throughout the Periodic Table. This discrepancy may be as large as 0.7 MeV for liquid-drop nuclei. Also, the three-quadratic-surface shape parametrization may only be used for axially symmetric shapes.

### F. Solution of the equilibrium condition

I write the potential energy of an arbitrary rotating nucleus with respect to the nonrotating sphere as

$$V(q)=E_s^{(0)}\{B_s(q)-1+2x[B_C(q)-1]+yB_R(q)\}\ , \tag{29}$$

where

$$B_s(q)=(E_n+1-E_n^{(0)})/E_s^{(0)}\ , \tag{30}$$

$$B_C(q)=B_C^{\rm sharp}+\Delta B_C\ , \tag{18}$$

$$B_R(q)=\left[\frac{15}{8\pi}d^3r\int r_1^2+10\left[\frac{a_M}{R_0}\right]^2\right]^{-1}\ , \tag{31}$$

$$x=\frac{a_C}{2c_s}\frac{Z^2}{A}\ , \tag{32}$$

and

$$y=\frac{5}{4}\frac{L^2\hbar^2}{M_0E_s^{(0)}R_0^2}\ . \tag{33}$$

The units $R_0$, $M_0$, and $E_s^{(0)}$ are defined by Eqs. (1), (2), and (16). The diffuseness-corrected Coulomb-energy constant is[17]

$$a_C=\frac{3}{5}\frac{e^2}{r}g(a_c/R_0)\ , \tag{34}$$

where

$$g(w)=1-5w^2[g_1(w)-\tfrac{3}{4}g_2(w)e^{-2/w}]\ , \tag{35}$$

$$g_1(w)=1-\tfrac{15}{8}w+\tfrac{21}{8}w^3\ , \tag{36}$$

and

$$g_2(w)=1+\tfrac{9}{2}w+7w^2+\tfrac{7}{2}w^3\ . \tag{37}$$

In contrast to the liquid-drop model, where results can be expressed entirely in terms of the two parameters $x^{\rm LD}$ and $y^{\rm LD}$, the results here depend explicitly on $Z$, $A$, and $L$. This is because of the occurrence in this model of the fixed ranges $a$, $a_c$, and $a_M$ which introduce nonanalytic behavior (as a function of $A$) into $B_s$, $B_C$, and $B_R$. It is sometimes convenient to present results as a function of $A$ only; for this purpose, when I refer to beta-stable nuclei, I shall mean nuclei whose charge and mass are related by Green's approximation to the line of beta stability[26]

$$Z=\frac{A}{2}\left[1-\frac{0.4A}{A+200}\right]\ . \tag{38}$$

The condition of equilibrium is

$$\frac{\partial V(q)}{\partial q_i}=0\ \ (i=1,\ldots,N_c)\ . \tag{39}$$

The character of the equilibrium point is determined by the signs of the eigenvalues of the curvature tensor

$$K_{ij}=\frac{\partial^2V(q)}{\partial q_i\partial q_j}\ . \tag{40}$$

If I denote the ordered eigenvalues of $K_{ij}$ by $\lambda_i$, a local minimum (e.g., a ground state) is defined by

$$\lambda_i>0\ \ (i=1,\ldots,N_c)\ , \tag{41}$$

while a saddle point is defined by

$$\begin{aligned}&\lambda_i<0\ \ (i\leqq\nu)\ ,\\ &\lambda_i>0\ \ (i>\nu)\ .\end{aligned} \tag{42}$$

The ordinary Bohr-Wheeler symmetric fission saddle-point shapes have $\nu=1$ for nuclei heavier than the Businero-Gallone transition point,[25,27,28] which is predicted to occur between $A=100$ and $A=140$. For the remainder of this paper, I will only consider mass-symmetric distortions, and saddle points with $\nu=1$. Mass-symmetric saddle points with $\nu>1$ do exist, but are of no physical relevance to binary fission.[20,29]

In order to solve Eq. (39), I perform a Taylor-series expansion of $V(q)$ in the vicinity of the equilibrium point, which has coordinates $\hat{\mathbf{q}}_i$

$$V(q)\sim V(\hat{\mathbf{q}})+\tfrac{1}{2}\sum_{i,j}K_{ij}(\hat{\mathbf{q}})(q_i-\hat{\mathbf{q}}_i)(q_j-\hat{\mathbf{q}}_j) \tag{43}$$

[since $(\partial V/\partial q_i)\,|_{\hat{\mathbf{q}}}=0$]. Differentiating with respect to the coordinates leads to

$$\frac{\partial V(q)}{\partial q_i}=K_{ij}(q)\Delta q_j+O(\Delta q^2)\ , \tag{44}$$

where

$$\Delta q_i\equiv q_i-\hat{\mathbf{q}}_i\ . \tag{45}$$

Equation (44) may be rewritten as

$$\hat{\mathbf{q}}_i=q_i-[K^{-1}(q)]_{ij}\frac{\partial V(q)}{\partial q_j}+O(\Delta q)\ . \tag{46}$$

With this vector version of Newton's root-finding method, a starting set of coordinates $q^{\rm I}$, in the neighborhood of $\hat{\mathbf{q}}$, when used to calculate $\partial V/\partial q$ and $K_{ij}$, will lead to a sequence of values $q^{\rm II},q^{\rm III},\ldots$, which will converge to $\hat{\mathbf{q}}$ as the number of iterations goes to infinity. Without attempting to make a mathematically precise definition of the extent of the neighborhood in which convergence occurs, I merely observe that convergence (to the intrinsic accuracy of $\partial V/\partial q_i$) usually occurs after about four or five iterations for an "average" case. For example, if the coordinates of an equilibrium-point shape for a certain nucleus with $A$, $Z$, and $L$ are used as the starting guess for a nucleus with $A+\Delta A$, $Z+\Delta Z$, and $L+\Delta L$, convergence will usually occur if $|\Delta A|\leqq 20$, $|\Delta Z|\leqq 5$, and $|\Delta L|\leqq 10$–$20$. Of course, in certain regions, such as near the maximum $L$ for which a minimum or a saddle point exists, shapes change more rapidly with $A$, $Z$, and $L$, and smaller increments must be used.

This technique for solving Eq. (39) allows a much more precise location of equilibrium points than many other

techniques, such as steepest-gradient methods. In addition, the calculation of the derivatives of $V(q)$ by quadrature, as is done here, leads to a much more accurate solution than is the case when these derivatives are calculated by numerical difference techniques. In Appendix B, I discuss in more detail the accuracy of the calculations and the convergence of the results with $N_c$ and quadrature order.

## III. QUALITATIVE RESULTS

The qualitative characteristics of the rotating ground states and saddle points in this work are similar to those of the rotating-liquid-drop model, which have been discussed in Ref. 1. I will briefly review these characteristics below.

### A. Nonrotating nuclei

For all nonrotating beta-stable nuclei with mass numbers less than about 300, the macroscopic ground state is a sphere. As one distorts the sphere with axially symmetric prolate distortions, the energy increases, until the fission saddle point is reached. Inside this saddle point, the net forces due to Coulomb repulsion and nuclear attraction tend to push the nucleus back to a spherical shape, while outside it, the forces tend to cause the nucleus to separate into fragments. For very heavy nuclei, the saddle point occurs at a very slight, almost spheroidal distortion, while the degree of distortion increases as one considers lighter and lighter nuclei. Somewhere in the vicinity of $A=240$, the saddle point shape makes a smooth transition from a cylinderlike shape to a necked-in dumbbell-like shape. For very light nuclei, the saddle-point shape corresponds to two almost-spherical nuclei attached by a small neck. All these saddle-point shapes are symmetric about their respective axes of maximum elongation. In Fig. 1, I show the shapes of selected nonrotating fission saddle points for beta-stable nuclei as a function of $A$ in the liquid-drop model, and in the present finite-range model. The shapes are scaled so that $R_0$ is the same for each nucleus. The primary noticeable differences between the shapes for the two models are smaller neck radii and slightly more elongation in the liquid-drop model.[18]

In Fig. 2, I show the calculated energies of the saddle points as a function of $A$ for beta-stable nuclei. The liquid-drop results in this figure are calculated using the same parametrizations and methods as those in the finite-range model, but using Eqs. (1)–(13) instead of Eqs. (15)–(19). The finite-range results are significantly lower in energy than those of the liquid drop model for $A \leq 200$, while very similar for $A > 200$.[18] Also, the maximum in the barrier height occurs at a larger value of $A$ in the finite-range model than in the liquid-drop model. The present results are qualitatively similar to those of Ref. 21, which used the same physical ingredients as the present work, but a different mathematical description of nuclear shapes. Figures 3 and 4 show the overall behavior of the barrier heights as a function of $Z$ and $A$ for nonrotating nuclei.

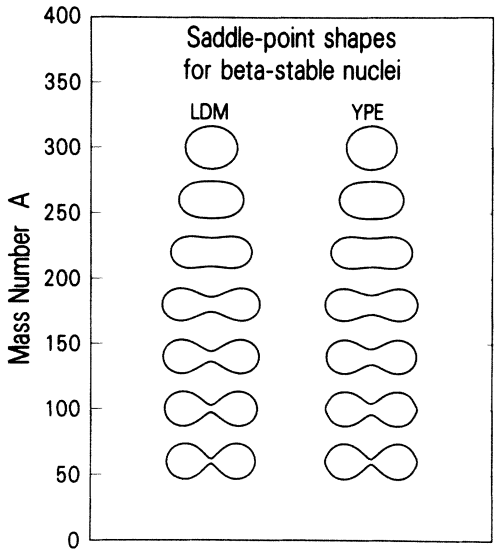


FIG. 1. Shapes of saddle points in the liquid-drop model and in the Yukawa-plus-exponential finite-range model for mass numbers $A$ from 60 to 300 in steps of 40. The value of the charge for each nucleus is determined from Green's approximation to the line of beta stability (Ref. 26). The closed curves are the intersections of the nuclear surface functions with planes through the axes of symmetry. The shapes are drawn with $R_0$ scaled to be the same for each nucleus.

### B. Rotating nuclei

If one considers a particular nucleus and the changes that occur as one increases the total angular momentum $L\hbar$ from zero, the ground state, which is initially spherical, becomes deformed into a nearly spheroidal oblate shape which is symmetric about the axis of rotation. As $L$ increases further, the stable ground state deforms further until, at a critical value $L_I$, the shape loses stability against a triaxial deformation mode. For nuclei with $A \leq 200$ (see Appendix C), there exists a stable triaxial

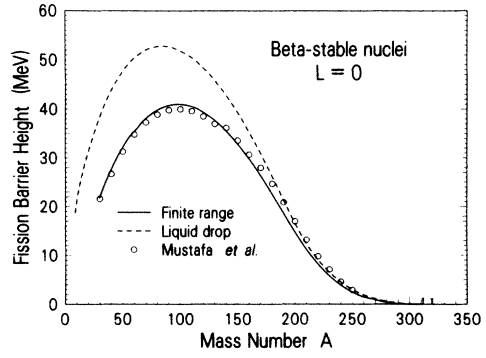


FIG. 2. Calculated fission barrier heights as a function of mass number for beta-stable nuclei in the liquid-drop and finite-range models (dashed and solid lines, respectively). The arrows show the predicted points at which the barriers completely disappear. The open circles are results from Ref. 21, which used the same finite-range energy functionals as in this work, but with a more restricted shape parametrization.

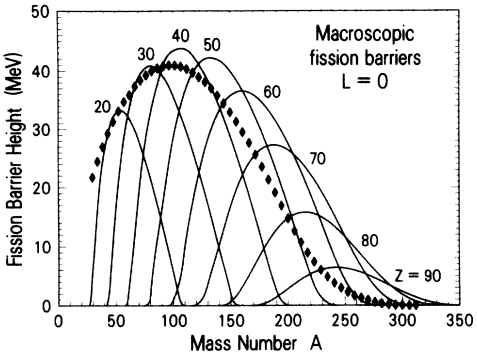


FIG. 3. Calculated fission-barrier heights as a function of mass number for atomic numbers $Z=20$ to 90. The points are barriers for beta-stable nuclei from $Z=14$ to $Z=117.9$ in steps of 2 (except for the last step). The points are the same as the solid curve in Fig. 2.

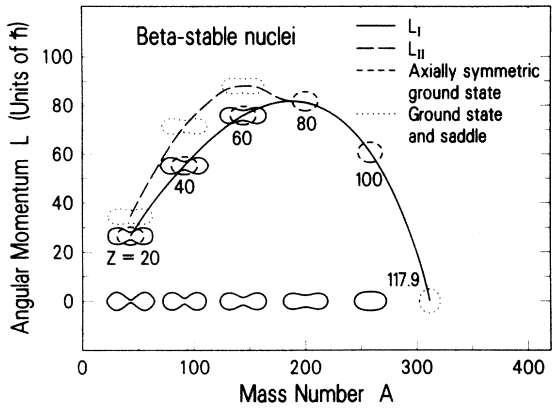


FIG. 5. Ground-state and saddle-point shapes as a function of mass number and angular momentum for beta-stable nuclei. The dashed shapes are axially symmetric ground states. The solid shapes are saddle points; those at $L=0$ are axially symmetric, while those at $L_I$ are slightly triaxial. The dotted shapes are those at the points where the ground-state family and the saddle-point family coalesce and the barrier vanishes. The shapes for $L_I$ at $Z=80$ and 100 are shown dashed to show that the fission barrier disappears at a symmetric shape. The right-hand dotted shape indicates the spherical nucleus with $Z=117.88$, $A=311.71$ whose macroscopic barrier vanishes at $L=0$.

ground-state family for $L>L_I$, which quickly goes from an oblate symmetric shape at $L_I$ to a prolate shape whose two larger moments of inertia are not greatly different from each other. As $L$ is increased further, the prolate shape continues to elongate until at $L_{II}$ it loses stability to fission. For $L>L_{II}$, no equilibrium shape exists, and a system with this much angular momentum cannot exist quasistatically in an undisintegrated configuration. For nuclei with $A>200$, the transition at $L_I$ is to a loss of stability to the same triaxial mode, but in this case no triaxial ground state exists and the triaxial deformation leads inexorably to fission for $L>L_I$.

For saddle points, increasing $L$ has approximately the same effect as increasing $x$; that is, the maximum elongation decreases, while the neck radius increases. In addition, a slight triaxiality occurs for nonzero $L$; this triaxiality never becomes very large except for very heavy nuclei for $L$ values near $L_I$. For $A\leqq 200$, as $L$ increases the elongation decreases until the neck is nearly cylindrical. At $L=L_{II}$, the shape becomes identical to the prolate triaxial ground-state shape described above, and the fission barrier disappears. Nuclei with $A>200$, which have cylinderlike or spheroidlike saddle-point shapes at $L=0$, have a symmetry axis perpendicular to the incipient axis of rotation. As $L$ increases, the major axis length shortens, while the minor axis length perpendicular to the rotation axis lengthens until the two become exactly equal at $L=L_I$, where the barrier and the ground-state family again disappear. In Fig. 5, I show the values of $L_I$ and $L_{II}$ as a function of $A$ for beta-stable nuclei. There are also several representative shapes shown. The shapes with solid outlines are saddle-point shapes at $L=0$ and $L=L_I$. The dashed shapes are the axially symmetric ground-state shapes at $L_I$ when the triaxial instability just sets in, while the dotted shapes are the shapes where the ground-state family and the saddle-point family coalesce. For all shapes with nonzero $L$, the axis of rotation is vertical. The shapes at $L_I$ for $Z=80$ and $Z=100$ are drawn dashed to emphasize that the barrier vanishes at an axially symmetric oblate configuration for heavy nuclei.

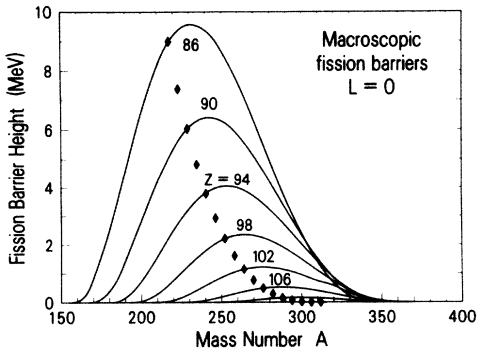


FIG. 4. Same as Fig. 3 for $Z=86$ to 110.

The values of $L_I$ and $L_{II}$ are also shown in Fig. 6, where they are compared to results from Ref. 1. Again the results of the two models are qualitatively similar to each other, with the value of $L_I$ being almost identical for $A\leqq 150$.

The dashed curves and the open diamond in Fig. 6 are taken directly from Ref. 1, while the open circle is an improved value calculated for the point of the disappearance of the triaxial ground state in the liquid-drop model (see Appendix C). In Fig. 7, I show the height of the fission barrier at $L=L_I$, where the triaxial ground state first appears. The difference of almost a factor of 2 between the two models indicates that formation and subsequent quasistability of superdeformed ground states, as predicted in Ref. 1 is very unlikely. This is an example of how the improved quantitative predictions of the finite-range-

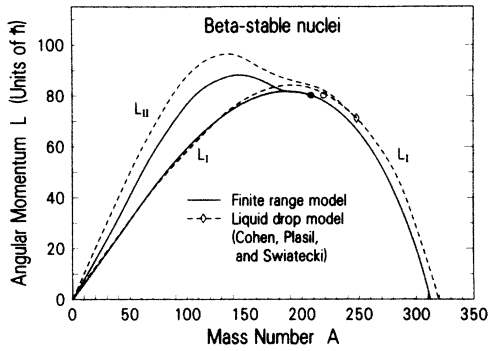


FIG. 6. $L_I$ and $L_{II}$ as a function of $A$ for beta-stable nuclei in the liquid-drop (Ref. 1) and finite-range-energy models. The open diamond is the previously reported point where $L_I(A)=L_{II}(A)$ (Ref. 1), while the open circle is the point calculated here for the liquid-drop model. The solid circle is the corresponding point for the finite-range model (see Appendix C).

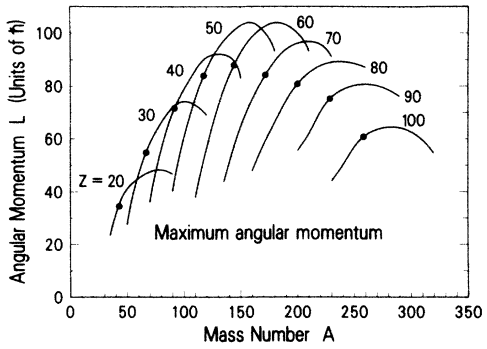


FIG. 8. Angular momentum at which the saddle point disappears and the barrier height goes to zero as a function of $A$ for $Z=20$ to 100. The curves for $Z=20$ to 70 are $L_{II}(A)$, while those for $Z=90$ and 100 are $L_I(A)$. The curve for $Z=80$ is for either $L_{II}$ or $L_I$, depending on the value of $A$. The solid points indicate beta-stable nuclei.

energy model can lead to significant differences in qualitative predictions.

In Fig. 8, I show the maximum angular momentum as a function of $Z$ and $A$. The points refer to beta-stable nuclei, and lie on the upper solid curve of Fig. 6.

Calculated fission-barrier heights as a function of angular momentum are shown in Figs. 9 and 10 for selected beta-stable nuclei with atomic numbers from 20 to 100.

## IV. DETAILED RESULTS

### A. Results for selected nuclei

Calculated fission barriers as a function of angular momentum are shown for the nuclei $^{97}$Rh, $^{153}$Tb, $^{176}$Os, and $^{229}$Np in Figs. 11 and 12. These particular nuclei are chosen to demonstrate the variation in behavior across the Periodic Table and because of previous experimental[3,5,8,9,15] and theoretical[21] investigations of the first three of these nuclei. The present calculations are similar to those of Ref. 21 for $^{97}$Rh, but can differ by almost 3 MeV for $^{153}$Tb and $^{176}$Os. Differences of this magnitude affect the degree to which experimental data on fission and evaporation-residue cross sections can be reproduced by statistical evaporation models.[14] In Figs. 13–16, I show the calculated moments of inertia for the ground states and for the saddle points as a function of $L$ for the same four nuclei. The moments of inertia are all expressed as ratios to that of a rigidly rotating, sharp-surfaced sphere

$$I_0=\tfrac{2}{5}M_0R_0^2\ . \tag{47}$$

This ratio is larger than 1.0 for the nonrotating spherical ground states due to the effect of the finite diffuseness of the matter distribution. Two striking results seen in these figures are that the triaxiality of the saddle-point shape is so slight that it is not discernable, except in the case of $^{229}$Np (Fig. 16) and the very rapid approach of the triaxial ground state to a prolate shape with $I_{max}\cong I_{mid}$ for $L>L_I$ (Figs. 13 and 14).

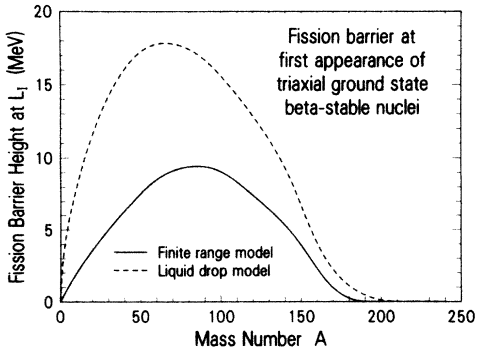


FIG. 7. Calculated height of the fission barrier at $L=L_I(A)$, where the triaxial instability of the ground state first appears, for beta-stable nuclei.

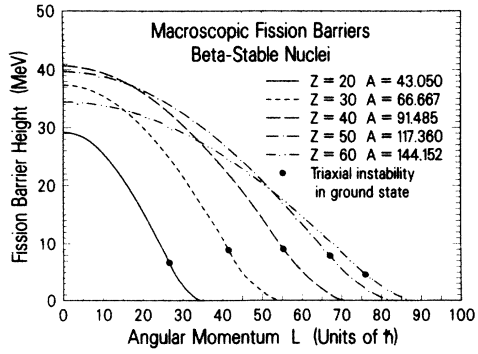


FIG. 9. Fission barrier heights as a function of angular momentum for beta-stable nuclei of atomic numbers $Z=20$ to 60. The solid circles represent the points at which the ground state changes from axially symmetric at lower values of $L$ to triaxial for higher values of $L$.

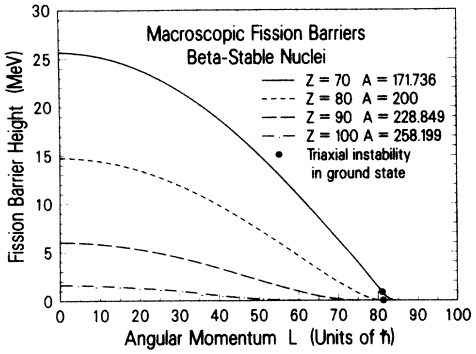


FIG. 10. Same as Fig. 9 for $Z=70$ to 100. There are no solid points for $Z=90$ and $Z=100$ since no triaxial ground states exist for these nuclei.

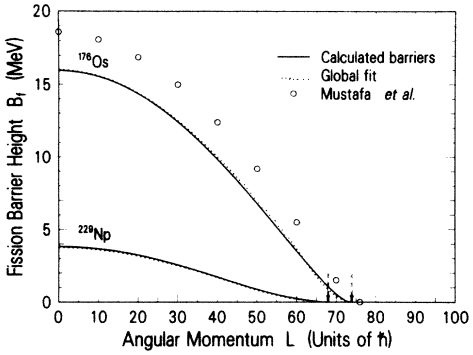


FIG. 12. Same as Fig. 11 for $^{176}$Os and $^{229}$Np. The results for $^{229}$Np were not tabulated in Ref. 21.

### B. Global approximation to barrier heights

Because the present results depend on the three variables $A$, $Z$, and $L$ and because experiments are becoming sensitive to predicted variations of the order of 1 MeV,[5,7,9,10,14,16] it is necessary to find a simple representation of the results which may be useful in statistical evaporation models. Such models need to use fission barriers of many different nuclei at many different values of $L$.[3,5,9,10,16] I use the following form to represent the fission barrier heights

$$B_f(A,Z,L)=B_f^0(A,Z)h(Z,A,L)\ , \tag{48}$$

where

$$h(Z,A,L)=1+\delta_2L^2+\delta_3L^3\ \ (L\leqq L_{20})\ ,$$
$$=1+\gamma_2l^2+\gamma_3l^3+\gamma_4l^4+\gamma_5l^5\ \ (L\geqq L_{20})\ , \tag{49}$$

$l=L/L_{\max}$, the quantities $B_f^0$, $L_{\max}$, $L_{20}$, $L_{80}$, $\delta_i$, and $\gamma_i$ are functions of $Z$ and $A$, $L_{20}$ ($L_{80}$) is the value of $L$ where the calculated barrier height is 20% (80%) of $B_f^0$ (the barrier for $L=0$), and $L_{\max}$ is the value of $L$ for which the barrier disappears. The four quantities $B_f^0$, $L_{20}$, $L_{80}$, and $L_{\max}$ are approximated by fitting to calculated values functions of the form

$$p_m(Z,A)=\sum_{i=0}^{N_A-1}\sum_{j=0}^{N_Z-1}C_{ij}^{(m)}P_i(\eta)P_j(\mu)\ , \tag{50}$$

where $p_m$ represents $B_f^0$, $L_{20}$, $L_{80}$, or $L_{\max}$; $\eta=A/400$; $\mu=Z/100$; $P_k$ is an ordinary Legendré polynomial; and $N_A$ and $N_Z$ are the number of terms in the resulting $A$

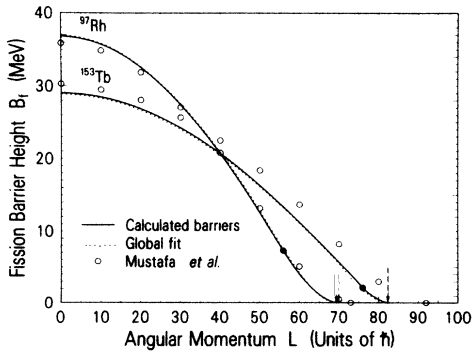


FIG. 11. Calculated fission barriers as a function of angular momentum for $^{97}$Rh and $^{153}$Tb. The solid lines are the present results, the dotted lines are from a global approximation to these calculations (see Sec. IV B), and the open circles are from the tabulated results of Ref. 21. The arrows and the right-most open circles correspond to the value of $L$ at which the barrier vanishes.

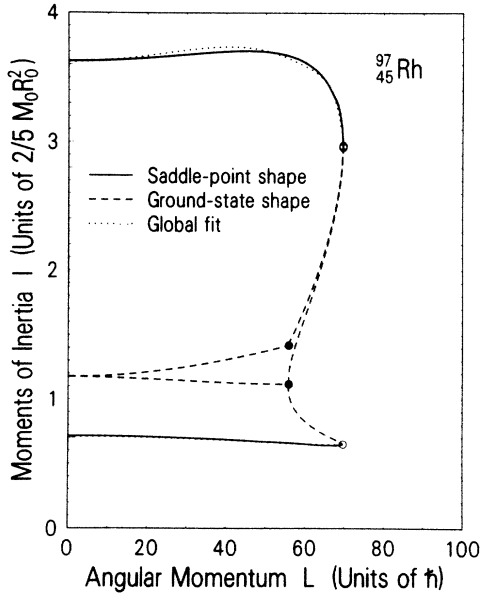


FIG. 13. Calculated rigid-body rotational moments of inertia for the ground-state and saddle-point families as a function of angular momentum for $^{97}$Rh. The solid lines give the moments of inertia for the saddle-point family, while the dotted lines are a global approximation to the calculated ones (see Sec. IV C). The dashed lines give the moments of inertia for the ground state family. The solid circles indicate where the triaxial ground-state transition occurs, while the open circles indicate where the barrier to fission vanishes.

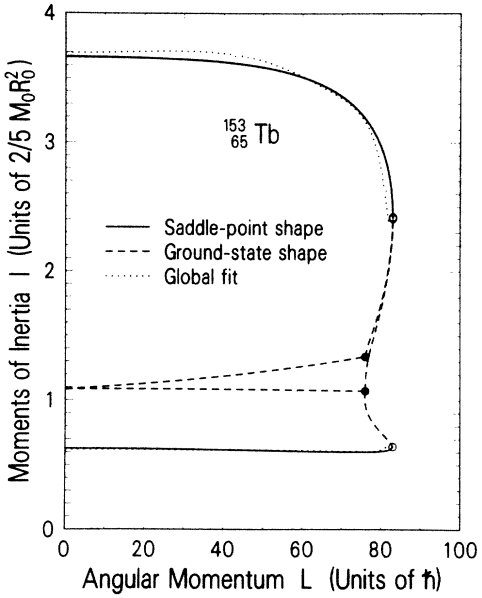


FIG. 14. Same as Fig. 13 for $^{153}$Tb.

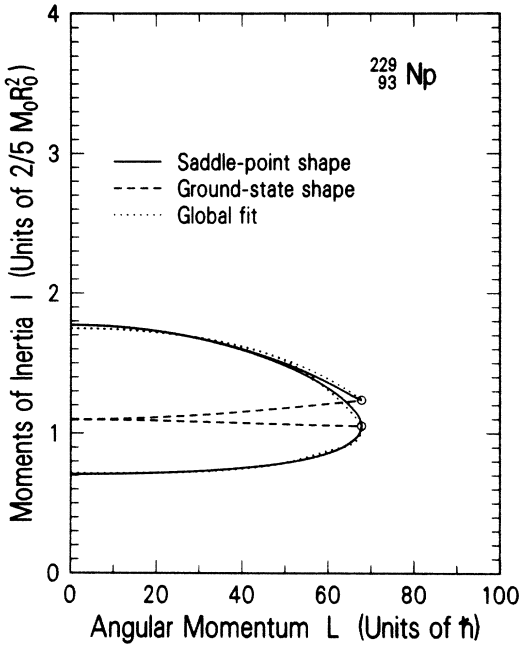


FIG. 16. Same as Fig. 13 for $^{229}$Np. This nucleus has no triaxial ground state.

and $Z$ series for fixed $Z$ and $A$, respectively ($N_Z$ is not the same as the quantity in Sec. II). The values of $\delta_i$ and $\gamma_i$ are expressible in terms of the last three of these $p_m$'s (see Appendix D).

The accuracy with which calculated barriers are approximated by this method may be inferred from the dotted lines in Figs. 10 and 11; these four nuclei were NOT included in the fits of any of the coefficients.

Because of the large number of coefficients $C_{ij}^{(m)}$ and the number of significant digits needed to accomplish this global fit, they are not given here. I have written a Fortran 77 computer subroutine called BARFIT which will calculate the height of the barrier and the energy of the ground state for given values of $Z$, $A$, and $L$ using the approximate methods discussed above and in Appendix D. Copies of this code are available from the National Energy Software Center.[34]

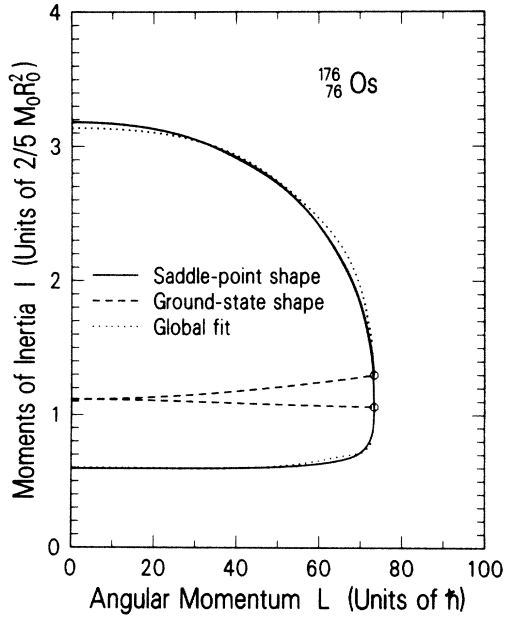


FIG. 15. Same as Fig. 13 for $^{176}$Os. This nucleus is near the critical point where $L_{\rm I}=L_{\rm II}$ and has no triaxial ground state.

### C. Global approximations to saddle-point moments of inertia

Just as fission-barrier heights are necessary for the calculation of fission and evaporation-residue cross sections, so are moments of inertia necessary for calculations of fission-fragment angular distributions.[30–32] I approximate the calculated moments of inertia with the functions of the form

$$I(Z,A,L)=\begin{Bmatrix} I_0+al^2+bl^4\equiv I_1(l) & l\leq 0.7 \\ I_1\cos^2\alpha+I_2\sin^2\alpha & 0.7<l<0.95 \\ I_1\cos^2\beta+I_2\sin^2\beta & 0.95\leq l\leq 1 \end{Bmatrix}, \quad (51)$$

where $I_0\equiv I(l=0)$,

$$I_2=I_0+[I(l=1)-I_0]e^{\gamma(l-1)}, \quad (52)$$

$\alpha=\pi(l-0.7)$, and $\beta=5\pi(l-0.95)$. The coefficients $a$ and $b$ are chosen so that $I_1$ equals the calculated moments for $l=0$, 0.7, ad 0.95. Expressions for $\gamma$, $a$, and $b$ are given in Appendix D. These quantities are defined in terms of $I_0$, $I_{70}$, $I_{95}$, and $I_{\rm max}$, the calculated values of the moments at $l=0$, 0.7, 0.95, and 1.0, respectively.

These four moments are approximated by functions of $Z$ and $A$ of the same form as Eq. (50) with $N_z=6$ and $N_A=5$. An additional complication is necessary in fitting $I_{\rm max}$ for $Z\geq 80$, since the shape at $l=1$ is an axially symmetric oblate shape. This additional modification is discussed in Appendix D. A computer subroutine named

MOMFIT is also available from the National Energy Software Center.[34] MOMFIT will calculate $L_{\max}$ and the three principal-axis moments of inertia of the saddle-point shape of a nucleus with given values of $Z$, $A$, and $L$. The degree of reproduction of the calculated moments of inertia by this method may be seen by referring to the dotted curves in Figs. 13–16. As in the preceding subsection, these four nuclei were NOT used in the fit of the coefficients $C_{ij}^{(m)}$ (see Appendix D).

## V. DISCUSSION AND SUMMARY

I have presented a macroscopic model for the free energy of rotating nuclei which has four major improvements relative to the rotating-liquid-drop model:

(1) replacement of surface tension energy with the double volume integral of an empirical finite-range Yukawa-plus-exponential two-body potential,[18]

(2) calculation of Coulomb energies for nuclei with charge distributions with diffuse surfaces,[19]

(3) calculation of rigid-body rotational moments of inertia for nuclear matter distributions with diffuse surfaces,[19] and

(4) the constants of the model are taken from a semiempirical nuclear mass formula with a superior fit to nuclear ground-state masses and to fission barriers of nonrotating nuclei.[17]

In addition to these physical ingredients, which have been used previously,[21] this study utilizes a new triaxial shape parametrization and highly accurate numerical techniques for the calculation of details of the macroscopic potential-energy surface.

The barriers calculated in this model have been found to be within about 1 MeV (for the $L$ values which are sampled in such experiments) of those which optimally reproduce fission and evaporation-residue cross sections[9,10,12,14–16] for a variety of nuclei with masses of 150 to 200+. The experimental data[14,15] are better reproduced with the results of this model than with those of the liquid-drop model[1] or with those of Ref. 21. An extension of the present model[28] to the barriers to mass-asymmetric fission predicts values which are within about 2 MeV of experimentally deduced ones for In nuclei.[33] Also, the moments of inertia calculated in this model, when included in a statistical transition-state model,[32] reproduce observed fission-fragment angular distributions for a variety of nuclei with masses of 160–250, for all cases where the transition-state picture predicts that the angular distributions are determined by the moments of inertia of the saddle-point shapes.

Several effects which have not been included may possibly be detectable (or ruled out) by experiments which are sensitive to fission barriers at different nuclear temperatures and values of $L$. These neglected effects include a temperature dependence of the nuclear-radius and surface-diffuseness constants and an angular-momentum dependence of the diffuseness. Similarly, single-particle effects as a function of angular momentum may be detectable by comparisons to the present model.

The results of calculations involving many hundreds of nuclei have been approximated in a useable form in two computer subroutines which will give accurate values for $L_{\max}$, $B_f(L)$, and the saddle-point moments of inertia of any measurable nucleus with $20 \leqq Z \leqq 100$.

## ACKNOWLEDGMENTS

I am grateful for the enlightenment resulting from conversations with M. Blann, H. C. Britt, K. T. R. Davies, J. L. C. Ford, A. Gavron, J. R. Leigh, P. Möller, M. G. Mustafa, F. Plasil, R. G. Stokstad, and W. J. Swiatecki. The continuing advice and support of J. R. Nix has been invaluable. This research was supported by the U.S. Department of Energy under a contract with the University of California and Contract DE-AC05-840R21400 with the Union Carbide Corporation.

## APPENDIX A: ENERGIES AND DERIVATIVES

The surface of a triaxial nucleus is defined in cylindrical coordinates by

$$\rho_s(z,\phi)=\rho_s^0(z)\eta(\phi)/\lambda \ , \tag{25}$$

where

$$(\rho_s^0)^2=\sum_k a_{2k}[P_{2k}(x)-1] \ , \tag{24b}$$

$$\eta(\phi)=1+\alpha_1 P_2(\cos\phi)+\alpha_2 P_4(\cos\phi) \ , \tag{26b}$$

$$\lambda=1+\alpha_1/4+9\alpha_2/64 \ , \tag{27b}$$

$x=z/z_0$, and the vector

$$q_i=\{a_2,\ldots,a_{2N_z},\alpha_1,\alpha_2\} \ .$$

### A. Rotational energy

The rotational energy functional is

$$B_R=\frac{I_0}{I}=\left[\frac{15}{8\pi}\int d^3r\, r_\perp^2+\frac{10a_M^2}{R_0^2}\right]^{-1} \ , \tag{A1}$$

where $r_\perp$ is the perpendicular distance from a point in the nucleus to the axis of rotation. I will denote the first term in the parentheses of Eq. (A1) as $\frac{5}{2}I^{\rm sh}$ where $I^{\rm sh}$ is the moment of inertia of a sharp-surfaced nucleus.

$$I_i^{\rm sh}=z_0^2\left[\tfrac{1}{3}+\frac{a_2 z_0}{5}\right](1-\delta_{i3})+\frac{1}{2\lambda^2}\left[\frac{3z_0}{4}\sum_k\frac{a_{2k}^2}{2k+1}-1\right]$$

$$\times[\theta_A(\delta_{i1}+\delta_{i3})+\theta_B(\delta_{i2}+\delta_{i3})] \ , \tag{A2}$$

where $i$ refers to one of the three Cartesian principal axes, $\delta_{ij}=1$ if $i=j$, and $\delta_{ij}=0$ if $i\neq j$,

$$\theta_A=1-\alpha_1/4-\alpha_2/32+5\alpha_1^2/32-43\alpha_1\alpha_2/512$$
$$+727\alpha_2^2/8192$$

and

$$\theta_B = 1 + 5\alpha_1/4 + 19\alpha_2/32 + 17\alpha_1^2/32 + 355\alpha_1\alpha_2/512 + 2847\alpha_2^2/8192 .$$

The first and second derivatives of $B_R$ with respect to $q_i$ are found by straightforward differentiation of Eqs. (A1) and (A2).

### B. Coulomb and nuclear energies

The Coulomb energy of a sharp-surfaced drop, the diffuseness correction to the Coulomb energy, and the Yukawa-plus-exponential nuclear energy are all double surface integrals of the form

$$\begin{Bmatrix} B_C \\ \Delta B_C \\ E_n/E_s^{(0)} \end{Bmatrix} = \oint\oint d\mathbf{S}\cdot\boldsymbol{\sigma}\, d\mathbf{S}'\cdot\boldsymbol{\sigma} g_m(\sigma) , \tag{A3}$$

where the symbols $d\mathbf{S}$, $d\mathbf{S}'$, and $\sigma$ are defined after Eq. (13),

$$g_1(\sigma) = -\frac{5}{64\pi^2\sigma} , \tag{A4}$$

$$g_2(\sigma) = \frac{15}{32\pi^2 a_c}\frac{1}{y_c^4}[2y_c - 5 + e^{-y_c}(y_c^2/2 + 3y_c + 5)] , \tag{A5}$$

where $y_c = \sigma/a_c$, and

$$g_3(\sigma) = -\frac{1}{8\pi^2 a^4 R_0^2}\frac{1}{y_n^4}[2 - e^{-y_n}(y_n^2 + 2y_n + 2)] , \tag{A6}$$

where $y_n = \sigma/a$. The other factors in Eq. (A3) may be written as

$$\oint d\mathbf{S}\cdot\boldsymbol{\sigma} = z_0 \int_{-1}^{1} dx \int_0^{2\pi} d\phi\, \rho \left[\rho - \rho' \left[\cos\Delta\phi + \frac{1}{\rho}\frac{\partial\rho}{\partial\phi}\sin\Delta\phi\right] - \Delta z\frac{\partial\rho}{\partial z}\right] \tag{A7}$$

and

$$\oint d\mathbf{S}'\cdot\boldsymbol{\sigma} = -z_0 \int_{-1}^{1} dx' \int_0^{2\pi} d\phi'\rho' \left[\rho' - \rho\left[\cos\Delta\phi - \frac{1}{\rho'}\frac{\partial\rho'}{\partial\phi'}\sin\Delta\phi\right] + \Delta z\frac{\partial\rho'}{\partial z'}\right] , \tag{A8}$$

where $x = z/z_0$, $\Delta z = z - z'$, and $\Delta\phi = \phi - \phi'$. The quantities $(\partial\rho/\partial z)$, $(\partial\rho/\partial\phi)$, etc., are calculated by differentiating Eq. (25) and using Eqs. (24b), (26b), and (27b). The integrals are approximated by use of Gaussian-Legendré quadrature. In subsequent discussions I will use the notation $N_g = (N_{gz}, N_{g\phi})$ to indicate a quadrature with $N_{gz}$ points on the $x$ interval $[-1,1]$ and $N_{g\phi}$ points on the $\phi$ interval $[0,\pi]$. Due to the symmetries of the shapes, the $x$ integral is actually performed only over the interval $[0,1]$, and the $\phi$ integral over $[0,\pi/2]$, while the $x'$ and $\phi'$ integrals cover the entire ranges specified in Eq. (A8).

First and second derivatives of the energy functionals with respect to the coordinates $q_i$ may be straightforwardly calculated by appropriately differentiating Eqs. (A3)–(A8), utilizing Eqs. (24)–(27b), and

$$\sum_k a_{2k} = -\frac{2}{3z_0} . \tag{A9}$$

Derivatives calculated by this method of applying numerical quadrature to the appropriate integral expressions have a much higher accuracy than achievable by use of numerical difference techniques.

## APPENDIX B: ACCURACY AND CONVERGENCE OF RESULTS

I discuss below results calculated by two different methods: the calculation for triaxial shapes detailed in Appendix A, and a calculation for axially symmetric shapes for which, because only two- and three-dimensional quadratures are done,[18,10] I may use a larger number of quadrature points than is practical for triaxial shapes. I have chosen to make detailed comparisons for the saddle point of the beta-stable nucleus $Z = 60$, $A = 144.152$, which has a typical well-deformed saddle-point shape characteristic of nuclei with $A \leq 180$. In Fig. 17, I show the relative error (compared to $N_c = 6$) in the saddle-point energy, the maximum elongation and the neck diameter for the $L = 0$ saddle point using the axially symmetric calculation, as a function of the number of shape coordinates employed, and in the three-quadrature-surface shape parametrization.[25]

The energy calculation is accurate to five parts in $10^6$ ($\sim 0.0002$ MeV) for $N_c \geq 5$. I have chosen to compare the results to those for $N_c = 6$ because in the finite-range model when $N_c \geq 7$ the saddle-point shape has extra unstable normal modes in addition to the one corresponding to fission. This is because the nuclear restoring force vanishes in the limit of small wavelength perturbations of the nuclear surface,[18] while the Coulomb force is always negative. The relative errors in all three plotted quantities for $N_c = 7$–$12$ vary in sign, with a maximum value of $5\times10^{-5}$ for the barrier height and a maximum of $10^{-2}$ for the geometrical quantities. The geometrical quantities plotted have the largest deviations; the rotational moments of inertia have relative errors more than an order of magnitude smaller than those shown. In Fig. 18, I show relative errors [with respect to $N_g = (256,64)$] as a function of quadrature order in both the axisymmetric and triaxial codes for a fixed number of degrees of freedom ($N_z = 5$). The axisymmetric calculation of the fission barrier has an accuracy which increases by about two orders of magnitude for each doubling of the number of integration points, while the accuracy of the triaxial calculations

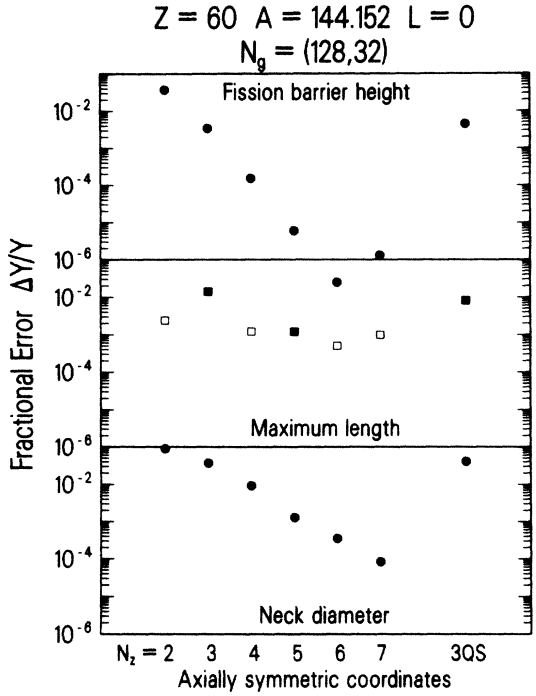


FIG. 17. Fractional error in the fission-barrier height, the maximum length, and the neck radius of the nonrotating saddle-point shape of $Z=60$, $A=144.152$ as a function of the number of independent coordinates used to describe the shape. The results are relative to those for $N_z=6$, $N_g=(128,32)$. For $N_z \geq 7$, shapes with spurious ripples and bulges appear. Solid symbols refer to positive discrepancies, while open symbols indicate negative discrepancies. The points at $N_z=6$ are estimated. 3QS refers to the three-parameter three-quadratic-surface parametrization (Ref. 25).

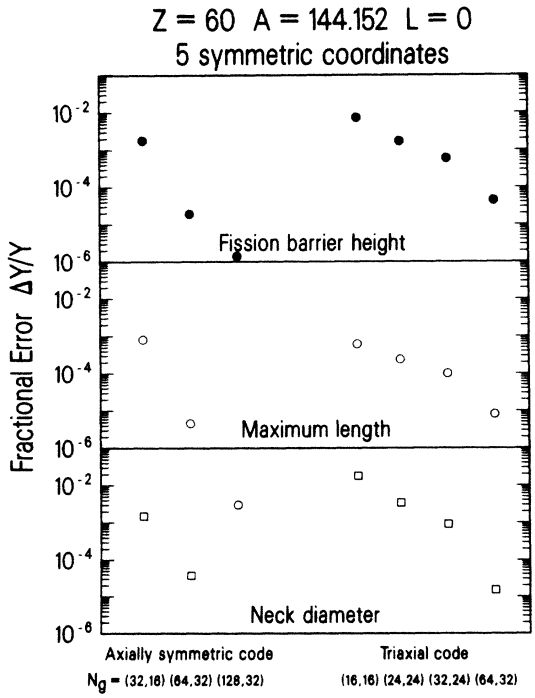


FIG. 18. Fractional errors as in Fig. 17 as a function of Gaussian quadrature order. The results are relative to $N_z=5$, $N_g=(256,64)$. Solid symbols indicate positive deviations, while open symbols indicate negative deviations.

improves by about one and a half orders of magnitude when doubling $N_g$. The calculations in the body of this paper for triaxial shapes use $N_c=7$, $N_z=5$, and $N_g=(32,24)$. Similar comparisons indicate that the error in the calculated value of $L_{\rm I}$ due to finite $N_z$ and $N_g$ is less than $0.02\hbar$, and the error in $L_{\rm II}$ is less than $0.2\hbar$.

## APPENDIX C: DISAPPEARANCE OF $L_{\rm II}$

In the region around $A=200$ for beta-stable nuclei, the potential-energy surface is relatively slowly varying for large changes in shape. This is the region where a relatively rapid transition occurs from spheroidlike saddle-point shapes for heavier nuclei to dumbbell-like shapes for lighter nuclei. This region is also where the existence of a triaxial ground state ceases as $A$ increases. Because of the "flatness" of the potential-energy surface, the fission barriers in the vicinity of this transition point are quite low, so the exact location of the point is not important with respect to observable properties of nuclei. However, the location of this transition point is of some mathematical interest and as the previously reported value for the liquid-drop model[1] is significantly in error, I present this appendix to describe the calculation of the point where the triaxial ground state vanishes as $A$ is increased.

First considering the liquid-drop model and following the notation of Ref. 1, I will let $y_{\rm I}(x)$ denote the value of $y$ at which the ground state loses stability to an axially asymmetric distortion. $y_{\rm II}(x)$ is the value of $y$ at which the triaxial ground state and the saddle point become identical and the fission barrier vanishes, while $y_c$ $(x_c)$ is the point at which the $y_{\rm II}$ function equals the $y_{\rm I}$ function. I will let $\epsilon_x \equiv x - x_c$ and $\epsilon_y \equiv y - y_{\rm I}(x)$. To lowest order in these quantities, the potential energy as a function of axial asymmetry $\alpha_1$ must have the form

$$V - V(x_c,y_c) = -A\epsilon_y\alpha_1^2 - B\epsilon_x\alpha_1^4 - C\alpha_1^6 , \tag{C1}$$

where $A$, $B$, and $C$ are positive constants. This equation is verified by noting that $V$ is symmetric about $\alpha_1=0$, has a local minimum at $\alpha_1=0$ and a local maximum at finite $\alpha_1$ for $\epsilon_y<0$, a local maximum at $\alpha_1=0$ for $\epsilon_y>0$, a local maximum and a local minimum at finite $\alpha_1$ for $\epsilon_x<0$, $\epsilon_y>0$, [for $y<y_{\rm II}(x)$], and no maxima or minima for finite $\alpha_1$ for $\epsilon_x>0$, $\epsilon_y>0$. In terms of these coefficients, when $\epsilon_x<0$ the triaxial ground state is located at

$$\alpha_1^2 = -\frac{B\epsilon_x}{3C}\left[1-\left[1-3\frac{AC}{B^2}\frac{\epsilon_y}{\epsilon_x^2}\right]^{1/2}\right], \tag{C2}$$

while the saddle point is located at

$$\alpha_1^2 = -\frac{B\epsilon_x}{3C}\left[1+\left[1-3\frac{AC}{B^2}\frac{\epsilon_y}{\epsilon_x^2}\right]^{1/2}\right]. \tag{C3}$$

For $\epsilon_x>0$, $\epsilon_y<0$, the saddle point is located by Eq. (C2), and there is no triaxial ground state. The function $y_{\rm II}(x)$ in the neighborhood of $x_c$ is defined by the vanishing of the quantity in parentheses;

$$y_{\rm II}(x) = y_{\rm I}(x) + \frac{B^2\epsilon_x^2}{3AC}, \quad x<x_c . \tag{C4}$$

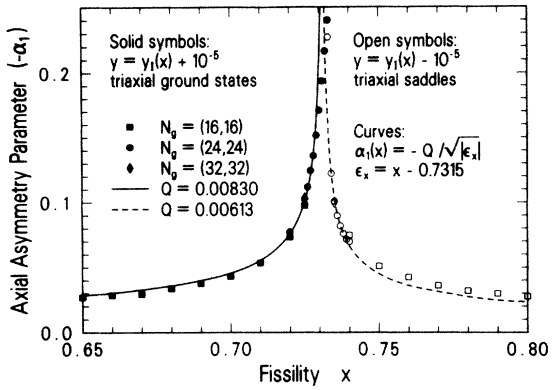


FIG. 19. Axial asymmetry parameter $(-\alpha_1)$ as a function of fissility for triaxial ground states (solid symbols) and saddle points (open symbols) in the rotating-liquid-drop model. The lines are arbitrarily normalized to the points in the vicinity of $\alpha_1=-0.1$.

For the present calculation, I first locate, using the methods of Sec. II, $y_I(x)$ in the vicinity of $x_c$; then I calculate the triaxial ground state for a fixed $\epsilon_y=10^{-5}$ as a function of $x$. Assuming with this choice that the last term in Eq. (C2) is much smaller than 1, the equation may be approximated by

$$|\alpha_1| \sim Q/|\epsilon_x|^{1/2}, \tag{C5}$$

where $Q=(A/2B)|\epsilon_y|$.

For $x>x_c$, a similar calculation is done, but here the saddle point for $\epsilon_y=-10^{-5}$ is calculated. In Fig. 19, I compare the values of $\alpha_1$ calculated for triaxial ground states and saddle points to curves of the form (C5). The calculations are performed with a rather coarse Gaussian quadrature mesh to locate the neighborhood of $x_c$, with more accurate calculations used to pinpoint $x_c$. The inverse-square-root dependence gives a reasonably good representation of the calculated points, when one realizes that the preceding discussion only considered lowest-order effects. The curves are arbitrarily normalized to give the correct magnitude in the neighborhood of $\alpha_1=-0.1$. The value of $x_c$ extracted in this manner is $x_c=0.7315\pm0.0010$, to be compared to the value $x_c\sim0.81$ reported in Ref. 1. For a beta-stable nucleus, this new value corresponds to $A=219.53$, $Z=86.79$, while the old result was $A\sim248$, $Z\sim97$.

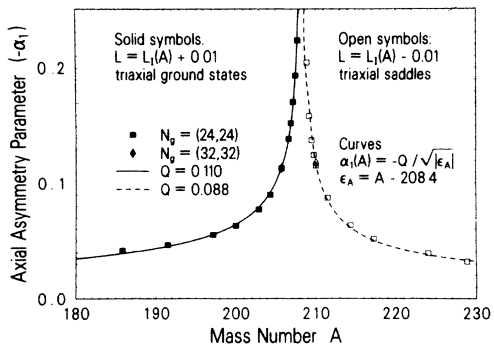


FIG. 20. Similar to Fig. 19 for the finite-range model, as a function of mass number $A$.

A similar calculation using the finite-range model is shown in Fig. 20. In this model, the critical point occurs for $A=208.4$, $Z=83.0$.

I would like to point out a possible reason why the earlier calculation gave a different result. As discussed above, the potential energy is *extremely* flat in the vicinity of $x_c$. A very small systematic error in the curvature $K_{ij}$ would cause a large displacement of the apparent location of $x_c$. The present calculations, with their careful evaluation of $K_{ij}$ are only practical with modern computers.

## APPENDIX D: GLOBAL APPROXIMATIONS TO BARRIERS AND MOMENTS OF INERTIA

### A. Fission barrier heights

The functional form of the global fit is defined by Eqs. (48)–(50). The functions $p_m$ are the following: $p_1=B_f^0$, $p_2=L_{\max}$, $p_3=L_{20}$, and $p_4=L_{80}$. The quantities $\delta_i$ and $\gamma_i$ in Eqs. (48) and (49) are related to the $p_i$'s by the following:

$$\delta_2=q(4p_4^3-p_3^3), \tag{D1}$$

$$\delta_3=-q(4p_4^2-p_3^2), \tag{D2}$$

$$q=\tfrac{1}{5}[p_3^2p_4^2(p_3-p_4)]^{-1}, \tag{D3}$$

$$\gamma_2=R(2l+1)(Vl_{80}-Wl_{20}), \tag{D4}$$

$$\gamma_3=-R[(2l_{80}+1)V-(2l_{20}+1)W]-2\gamma_2, \tag{D5}$$

$$\gamma_4=5\gamma_2-\gamma_3-5, \tag{D6}$$

$$\gamma_5=\gamma_3+2\gamma_2+4, \tag{D7}$$

$$V=l_{80}^2(l_{80}-1)(-20l_{20}^5+25l_2^4-4), \tag{D8}$$

$$W=l_{20}^2(l_{20}-1)(-20l_{80}^5+25l_{80}^4-4), \tag{D9}$$

$$R=\tfrac{1}{5}\{(l_{80}-l_{20})[l_{20}l_{80}(1-l_{20})(1-l_{80})]^2\}^{-1}, \tag{D10}$$

$$l_{20}\equiv p_3/p_2,$$

and $l_{80}\equiv p_4/p_2$.

$p_1$ is fit to 652 calculated barriers using $N_Z=N_A=7$ (49 coefficients $C_{ij}^{(1)}$. $p_2$ is fit to 61 calculated values of $L_{\max}$ using $N_Z=7$, $N_A=5$ (35 coefficients $C_{ij}^{(2)}$). $p_3$ and $p_4$ are fit to 36 calculated points using $N_Z=5$, $N_A=4$ (20 coefficients each in $C_{ij}^{(3)}$ and $C_{ij}^{(4)}$). The range of the $Z$ fit is from 20 to 110 for $p_1$, and from 20 to 100 for $p_2-p_4$. The range of $A$ values included for each $Z$ extends well beyond the range which could be of experimental interest.

### B. Moments of inertia

The three principal-axis moments of inertia are separately approximated by expressions of the form of Eqs. (51)–(52). For each of three Cartesian axes, I define the four quantities $p_5\equiv I$ $(l=0)$, $p_6\equiv I$ $(l=0.7)$, $p_7\equiv I$ $(l=0.95)$, and $p_8\equiv I$ $(l=1)$. In terms of these functions of $Z$ and $A$, which each have 30 coefficients ($N_Z=6$ and $N_A=5$),

$$a = -3.148\,85p_5 + 4.465\,06p_6 - 1.316\,21p_7 , \quad \text{(D11)}$$

$$b = 2.261\,29p_5 - 4.947\,43p_6 + 2.686\,14p_7 , \quad \text{(D12)}$$

and

$$\gamma = -20 \ln \left[ \frac{p_5 - p_7}{p_5 - p_8} \right] . \quad \text{(D13)}$$

For the moment of inertia $I_z$, $\gamma = 60$.

Because the shape at $L_{\max}$ ($l = 1$) is a symmetric oblate one for heavier nuclei (see Appendix C), the quantities $p_8$ for each of the three Cartesian axes are separately fit with 16 coefficients each for $Z \geqq 80$. The two larger moments of inertia $I_x$ and $I_y$ are approximated in this $Z$ region for all $l$ by functions of the form of $I_1(l)$ [see Eq. (51)] with the coefficients

$$a = 4.001\,60p_6 - 0.960\,78p_8 - 3.040\,82p_5 \quad \text{(D14)}$$

and

$$b = -4.001\,60p_6 + 1.960\,78p_8 + 2.040\,82p_5 . \quad \text{(D15)}$$

The smallest moment of inertia $I_z$ uses the complete form of Eq. (51) with the appropriate value of $p_8$ ($Z < 80$ or $Z \geqq 80$).

---

*Permanent address: Theoretical Division, Los Alamos National Laboratory, Los Alamos, NM 87545.

[1]S. Cohen, F. Plasil, and W. J. Swiatecki, Ann. Phys. (N.Y.) **82**, 557 (1974).

[2]W. D. Myers and W. J. Swiatecki, Ark. Fys. **36**, 343 (1967).

[3]M. Beckerman and M. Blann, Phys. Lett. **68B**, 31 (1977); Phys. Rev. Lett. **38**, 272 (1977); Phys. Rev. C **17**, 1615 (1978).

[4]G. Andersson., M. Areskoug, H.-Å. Gustafsson, G. Hyltén, B. Schrøder, and E. Hagebø, Z. Phys. A **293**, 241 (1979).

[5]F. Plasil, R. L. Ferguson, R. L. Hahn, Felix E. Obenshain, Frances Pleasonton, and G. R. Young, Phys. Rev. Lett. **45**, 333 (1980).

[6]W. von Oertzen, H. Fuchs, A. Gamp, H. Homeyer, U. Jahnke, and J. C. Jacmart, Z. Phys. A **298**, 207 (1980).

[7]M. Blann and T. T. Komoto, Phys. Rev. C **24**, 426 (1981); **26**, 472 (1982).

[8]B. Sikora, W. Scobel, M. Beckerman, J. Bisplinghoff, and M. Blann, Phys. Rev. C **25**, 1446 (1982).

[9]D. J. Hinde, J. R. Leigh, J. O. Newton, W. Galster, and S. Sie, Nucl. Phys. **A385**, 109 (1982).

[10]D. J. Hinde, J. O. Newton, J. R. Leigh, and R. J. Charity, Nucl. Phys. **A398**, 308 (1983).

[11]M. Blann, Phys. Rev. Lett. **49**, 505 (1982).

[12]F. Plasil, R. L. Ferguson, R. L. Hahn, Felix E. Obenshain, Frances Pleasonton, and G. R. Young, Phys. Rev. Lett. **49**, 506 (1982).

[13]F. D. Becchetti, H. H. Hicks, C. A. Fields, R. J. Peterson, R. S. Raymond, R. A. Ristinen, J. L. Ullmann, and C. S. Zaidins, Phys. Rev. C **28**, 1217 (1983).

[14]J. van der Plicht, H. C. Britt, M. M. Fowler, Z. Fraenkel, A. Gavron, J. B. Wilhelmy, F. Plasil, T. C. Awes, and G. R. Young, Phys. Rev. C **28**, 2022 (1983).

[15]F. Plasil, T. C. Awes, B. Cheynis, D. Drain, R. L. Ferguson, F. E. Obenshain, A. J. Sierk, S. G. Steadman, and G. R. Young, Phys. Rev. C **29**, 1145 (1984).

[16]K. T. Lesko, W. Henning, K. E. Rehm, G. Rosner, J. P. Schiffer, G. S. F. Stephans, B. Zeidman, and W. S. Freeman (unpublished).

[17]P. Möller and J. R. Nix, Nucl. Phys. **A361**, 117 (1981); At. Data Nucl. Data Tables **26**, 165 (1981).

[18]H. J. Krappe, J. R. Nix, and A. J. Sierk, Phys. Rev. Lett. **42**, 215 (1979); Phys. Rev. C **20**, 992 (1979).

[19]K. T. R. Davies and J. R. Nix, Phys. Rev. C **14**, 1977 (1976).

[20]S. Tentalange, S. E. Koonin, and A. J. Sierk, Phys. Rev. C **22**, 1159 (1980).

[21]M. G. Mustafa, P. A. Baisden, and H. Chandra, Phys. Rev. C **25**, 2524 (1982).

[22]K. T. R. Davies and A. J. Sierk, J. Comp. Phys. **18**, 311 (1975).

[23]W. D. Myers, Nucl. Phys. **A145**, 387 (1970).

[24]G. Süssmann, Z. Phys. A **274**, 145 (1975).

[25]J. R. Nix, Nucl. Phys. **A130**, 241 (1969).

[26]A. E. S. Green, *Nuclear Physics* (McGraw-Hill, New York, 1955), pp. 185, 250.

[27]U. L. Businaro and S. Gallone, Nuovo Cimento **1**, 629 (1955); **1**, 1277 (1955).

[28]K. T. R. Davies and A. J. Sierk, Phys. Rev. C **31**, 915 (1985).

[29]V. M. Strutinsky, N. Ya. Lyaschenko, and N. A. Popov, Z. Eksp. Teor. Fiz. **43**, 584 (1962) [Sov. Phys.—JETP **16**, 418 (1963)]; Nucl. Phys. **46**, 639 (1963).

[30]I. Halpern and V. M. Strutinsky, Proceedings of the U.N. International Conference on Peaceful Uses of Atomic Energy, 1955, Vol. 2, No. 15, p. 408.

[31]R. Vandenbosch and J. R. Huizenga, *Nuclear Fission* (Academic, New York, 1973), pp. 179ff.

[32]A. Gavron, P. Eskola, A. J. Sierk, J. Boissevain, H. C. Britt, K. Eskola, M. M. Fowler, H. Ohm, J. B. Wilhelmy, S. Wald, and R. L. Ferguson, Phys. Rev. Lett. **52**, 589 (1984).

[33]A. J. Sierk, Phys. Rev. Lett. **55**, 582 (1985).

[34]BARMOM, #9677, National Energy Software Center, Argonne National Laboratory, Argonne, IL 60439.